Research Article | Vol. 30, No. 19 / 12 Sep 2022 / Optics Express 34149
Optics EXPRESS

Optical bi-stability in cubic silicon carbide microring resonators

KEITH POWELL,[1,2] JIANFU WANG,[1] AMIRHASSAN SHAMS-ANSARI,[2] BIN-KAI LIAO,[1] DEBIN MENG,[1] NEIL SINCLAIR,[2,3] LIWEI LI,[1] JIANGDONG DENG,[4] MARKO LONČAR,[2,5] AND XIAOKE YI[1,*]

[1]School of Electrical and Information Engineering, Faculty of Engineering, The University of Sydney, NSW 2006, Australia
[2]John A. Paulson School of Engineering and Applied Sciences, Harvard University, 29 Oxford Street, Cambridge, MA 02138, USA
[3]Division of Physics, Mathematics and Astronomy, and Alliance for Quantum Technologies (AQT), California Institute of Technology, 1200 East California Boulevard, Pasadena, CA 91125, USA
[4]Center for Nanoscale Systems, Harvard University, Cambridge, MA 02138, USA
[5]loncar@seas.harvard.edu
[*]yi.xiaoke@sydney.edu.au

Abstract: We measure the photothermal nonlinear response in suspended cubic silicon carbide (3C-SiC) and 3C-SiC-on-insulator (SiCOI) microring resonators. Bi-stability and thermo-optic hysteresis is observed in both types of resonators, with the suspended resonators showing a stronger response. A photothermal nonlinear index of 4.02×10^{-15} m^2/W is determined for the suspended resonators, while the SiCOI resonators demonstrate one order of magnitude lower photothermal nonlinear index of 4.32×10^{-16} m^2/W. Cavity absorption and temperature analysis suggest that the differences in thermal bi-stability are due to variations in waveguide absorption, likely from crystal defect density differences throughout the epitaxially grown layers. Furthermore, coupled mode theory model shows that the strength of the optical bi-stability, in suspended and SiCOI resonators can be engineered for high power or nonlinear applications.

1. Introduction

Silicon carbide (SiC) is an emerging semiconductor material with the potential to fulfill many applications in integrated photonics. For instance, the SiC platform has shown promise for nonlinear optics [1–4], electro-optic modulation [5], opto-mechanics and quantum emitters [6–8]. The wide band-gap, high refractive index (~ 2.57), low thermo-optic coefficient [9], absence of two-photon absorption (TPA) at 1550 nm, and appreciable optical nonlinearities [1–5,10,11], make SiC ideal for a wide variety of linear and nonlinear optical applications.

Recently, the SiC optical platform has undergone rapid development and significant advancements have been made in optical quality (Q) factor of micro-resonators and nanophotonic cavities fabricated in SiC materials [1–5,9–15]. However, studies of optical bi-stability have not been extensively explored in SiC. High optical intensities within optical cavities can produce optical bi-stability or photothermal nonlinear response [16,17]. This is caused by a nonlinear change in the effective refractive index due to optical absorption and production of heat within the cavity. Enhancement of this effect can be useful for all-optical memory [18], photon-pair sources [19], switches, and logic gates [20,21], on the other hand, it can be desirable to minimize optical bi-stability for linear optical applications [22], such as microwave photonics [23,24] and programmable optical meshes [25]. While optical bi-stability has been broadly studied in other photonic integrated platforms [16–22,26,27], the observation of optical bi-stability in SiC has been limited to amorphous SiC [28] and 4H-SiC [29], and has not been rigorously

#469529 https://doi.org/10.1364/OE.469529
Journal © 2022 Received 4 Jul 2022; revised 13 Aug 2022; accepted 16 Aug 2022; published 2 Sep 2022

Optics EXPRESS

quantified. Among various polytypes of SiC, cubic (3C) SiC is the only polytype to exhibit intrinsically zero-birefringence and symmetrical electro-optic index ellipsoid with elements of the electro-optic tensor equal in magnitude [30]. This reduces complexities in optoelectronic integration and facilitated the demonstration of a Pockels modulator on 3C-SiC-on-insulator (SiCOI) [5]. Indeed 3C-SiC can be grown on silicon substrates with desired thickness and etched to create various microring resonators [5,9,31–33].

In this article, we fabricate, measure and quantify the photothermal nonlinear responses in suspended 3C-SiC and SiCOI resonators at telecommunication wavelengths. Coupled mode theory (CMT) is used to model the bi-stable behavior and quantify the photothermal nonlinear index, which determines the strength of the observed bi-stability. A photothermal nonlinear index of 4.02×10^{-15} m^2/W is obtained for the suspended resonator, which is higher than silicon (2×10^{-15} m^2/W) [34], whereas the SiCOI waveguide resonator has a photothermal nonlinear index of 4.32×10^{-16} m^2/W, which is around one order of magnitude lower than silicon. Cavity absorption and temperature analysis show the differences in thermal nonlinear index are expected to be caused by differences in optical absorption induced by polycrystalline domains [32] of the 3C-SiC substrate. Furthermore, the CMT model shows that the degree of bi-stability in suspended and SiCOI microring resonators can be tailored according to applications.

The optical waveguide structures enhance thermal nonlinear effects to yield measurable optical bi-stability. For this reason, we choose to fabricate microring resonators, which have a large optical field enhancement factor [35]. Each device consists of a ring resonator coupled to a bus waveguide where light is directed in and out via vertical grating couplers (VGCs). The coupling gaps between the resonators and bus waveguides are optimized to give a critical coupling condition to achieve the highest extinction ratio and maximal optical field enhancement factor. A rib waveguide design with a slab thickness of less than 135 nm is chosen to reduce the interaction between the optical mode and sidewalls of waveguides [36], while providing mechanical support to the suspended waveguide to facilitate photonic integration. The waveguide dimensions are determined by finite element method (FEM) simulations in COMSOL Multiphysics based on a maximum etch depth of 350 nm, and a sidewall angle of 75.6° which are constrained by the fabrication process. The 800 nm-width waveguides are chosen to allow minimal bending loss and single transverse electric (TE) mode operation, where the waveguide heights and slab thicknesses of suspended and SiCOI waveguides are shown in Figs. 1(a) and 1(b), respectively. Both devices are fabricated using a complementary metal-oxide-semiconductor (CMOS) foundry compatible process [5,9]. Both ring radii are set as 40 μm to minimize the bending loss [9]. The source wafer consists of 3C-SiC epitaxially grown on a silicon substrate with 3.5 μm of SiC epitaxially grown on silicon substrate. Due to the lattice mismatch between 3C-SiC and silicon, stacking faults occur at the growth interface. The grain boundaries are a source of optical scattering loss and absorption [9,32]. In SiCOI waveguides, a flip, bond and polish method is used to remove the stacking faults and anti-phase boundaries at the SiC-Si interface [5,32], whilst the suspended devices are required to be etched within high crystal defect density region as this region is closest to the underlying support provided by the silicon substrate [33]. In this work, the suspended 3C-SiC waveguides are surrounded by an air cladding formed by undercutting the silicon substrate of approximately 50 μm thickness (Fig. 1(a)). To ensure sufficient optical absorption to probe the thermo-optic bi-stability at low power levels, no thermal annealing is applied to the suspended chip [9]. On the other hand, the SiCOI waveguides are wrapped by oxide cladding with a top oxide thickness of 1 μm, and a bottom oxide thickness of 2 μm. Scanning electron microscopy (SEM) images of the fabricated suspended and SiCOI resonators and VGCs are, respectively, shown in Figs. 1(c)-(d) and Figs. 1(e)-(f).

Before measuring bi-stability, the spectral response of each resonator is determined by varying the wavelength of a laser beam that is directed to the VGC. The recorded spectral responses for representative suspended and SiCOI resonators are shown in Figs. 2(a) and 2(b), respectively.

Optics EXPRESS

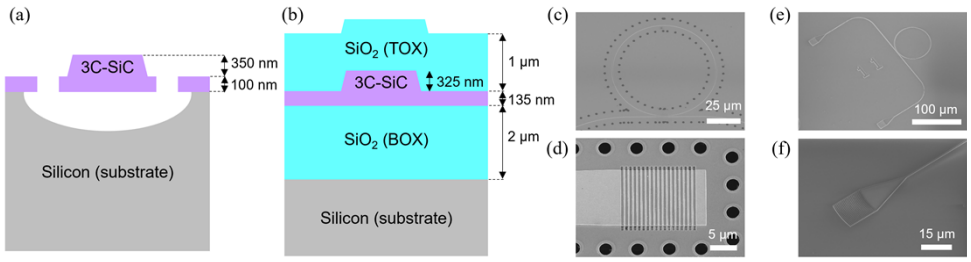

Fig. 1. (a) Schematic diagram of the suspended 3C-SiC waveguide cross section, with dimensions. (b) Schematic diagram of the 3C-SiCOI waveguide cross section showing top oxide (TOX) and bottom oxide (BOX) cladding, with dimensions. Scanning electron micrographs of (c) the fabricated suspended ring resonator (d) vertical grating coupler used to couple light into the suspended cavity (e) the fabricated 3C-SiCOI ring resonator and (f) vertical grating coupler of 3C-SiCOI waveguide.

The data reveals single mode operation with free spectral ranges (FSRs) of 3.35 nm and 3.26 nm, respectively, as per design and a close to critically coupled condition for SiCOI resonator. The small difference in FSR is due to the difference in group index as a result of differing waveguide dimensions and claddings for the suspended and SiCOI cavities. The intrinsic Q (Q_I) for each device is measured using Lorentz fitting of the optical resonance by measuring its transmission spectrum. A 240 pm full-width-half-maximum (FWHM) linewidth is measured for an under-coupled suspended microring resonator. This corresponds to a Q_I value of 9,500 (Fig. 2(a)), which indicates a linear propagation loss of around 52 dB/cm. Due to improvement in 3C-SiC crystallinity for the SiCOI resonators, the SiCOI resonator has a narrower linewidth of 144 pm, corresponding to a Q_I value of 23,000 (Fig. 2(b)) and a linear propagation loss of about 20 dB/cm. The propagation loss in SiCOI waveguide can be reduced by optimizing the SiC waveguide geometry, which results in improved mode confinement and less scattering due to reduced optical mode and sidewall interaction. The analysis of the waveguide surface roughness can be used to evaluate the scattering loss [32].

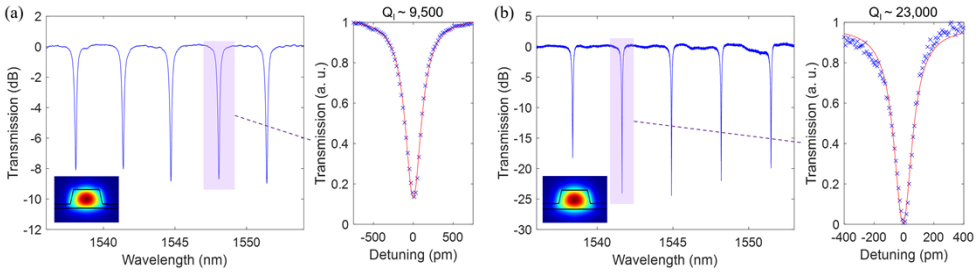

Fig. 2. (a) Optical transmission spectrum of a suspended single mode cavity and Lorentz fit of the resonant mode to determine the intrinsic optical quality factor (Q_I) (Cross: Measurement; Solid line: Lorentz fitting). Inset: Optical mode profile of the suspended cavity (largest intensity in dark red) (b) Optical transmission of the SiCOI ring cavity and Lorentz fit of the resonant mode to determine Q_I (Cross: Measurement; Solid line: Lorentz fitting). Inset: Optical mode profile for the SiCOI cavity (largest intensity in dark red).

Optics EXPRESS

2. Measurement of optical bi-stability

The bi-stability of 3C-SiC is inferred by pumping the suspended and SiCOI microring cavities with increasing optical power. Accordingly, the microring resonators are pumped using light from a tunable laser. The wavelength of the light is scanned at a constant rate of 20 nm/s. This ensures the sweep time through the resonance is much longer than the thermal relaxation time of SiC, which is typically on the scale of microsecond [5]. Therefore, the local thermodynamic quasi-equilibrium is established during the sweep [37]. An erbium-doped fiber amplifier (EDFA) is used to increase the optical power launched into the resonators in steps of 100 mW. Figures 3(a) and 3(b) show the measured spectral responses of the suspended and SiCOI devices at various laser power levels, when varying the laser from shorter to longer wavelengths (red scan). As the input power incident to the VGC is increased, a redshift of the resonance is observed. The resonance spectra become increasingly asymmetric indicative of optical bi-stability attributed to the thermo-optic effect. The wide band-gap (~ 2.3 eV) [33] of SiC eliminates refractive index changes brought by TPA at telecommunication wavelengths (1550 nm ~ 0.8 eV) and free-carrier absorption. The transmission responses of these devices are also characterized when sweeping the laser from longer to shorter wavelengths (blue scan). The results shown in Figs. 3(c) and 3(d) indicate that the resonant wavelength shifts during the blue scan are smaller than that of the red scan for both platforms. This is due to the resonance wavelength varying with that of the laser during the red scan, while varying opposite to that of the laser during the blue scan. Hence, a smaller amount of heating is observed for the blue scan [16]. Calculated based on the transmission spectra in Figs. 3(a) and 3(b), the 3C-SiC resonators exhibit a resonance shift of 4.3 pm/mW and 0.42 pm/mW with varied laser power for the suspended and SiCOI platforms, respectively. The resonance shifts are dominated by the thermo-optic effect. The thermal expansion factor of SiC is on the order of 10^{-6} K^{-1} [38], which is one order of magnitude smaller than the thermo-optic coefficient of SiC and leads to a small contribution to the geometry change in the resonance shift. Moreover, the 3C-SiC resonators are surrounded by other parts of the chip that are not heated that could constrain thermal expansion effect [39]. Considering the power-induced resonance shift (r), resonance wavelength (λ), group refractive index (n_g), VGC loss (η), enhancement factor (F) defined as the intensity enhancement inside the microring resonator compared with the bus waveguide [35], and the effective mode area (A_{eff}) of these cavities, the thermal nonlinear indexes n_2 are, respectively, calculated to be 4.02×10^{-15} m^2/W and 4.32×10^{-16} m^2/W for suspended and SiCOI waveguides, where $n_2 = rn_gA_{eff}/(\eta\lambda F)$. The large n_2 observed in the suspended platform is likely caused by the aforementioned higher optical absorption due to dangling bonds [9,32] at the grain boundary interfaces in the SiC-Si defect layer.

The relationships between absorbed power and cavity stored energy for the 3C-SiC resonators in the red scan are plotted in Fig. 4(a), where the slopes of the linear fit lines represent the absorption rate (τ_l^{-1}) [40]. Due to the absence of TPA and FCA at telecommunication wavelengths, the linear absorption [40], accounting for both surface absorption and bulk absorption of the optical cavity [41], represents the primary factor contributing to the photothermal induced resonance shifts in SiC devices. For the suspended resonator, the measured absorption rate is 1.8 times higher than the SiCOI resonator. Moreover, by considering the thermal-optic effect within the 3C-SiC waveguides, we calculate the temperature increases of the resonators with cavity power by combining the electromagnetic and heat-transfer physics in a numerical model based on FEM [42]. The temperature increase has a good agreement with that predicted by simulation, as shown in Fig. 4(b). Consistent with the larger absorption rate, the suspended resonator exhibits a 9.7 times higher rate of temperature increase than the SiCOI resonator. The extracted thermal resistances (R) of the suspended and SiCOI waveguides are 3.85×10^3 K/W and 7.62×10^2 K/W, indicating the suspended waveguide has a higher rate of heating. Figures 4(c) and 4(d) show the simulated cross-sectional temperature distributions via FEM in these two waveguide platforms at the circulation power of 320 mW and 330 mW, respectively. The temperature of suspended

Optics EXPRESS

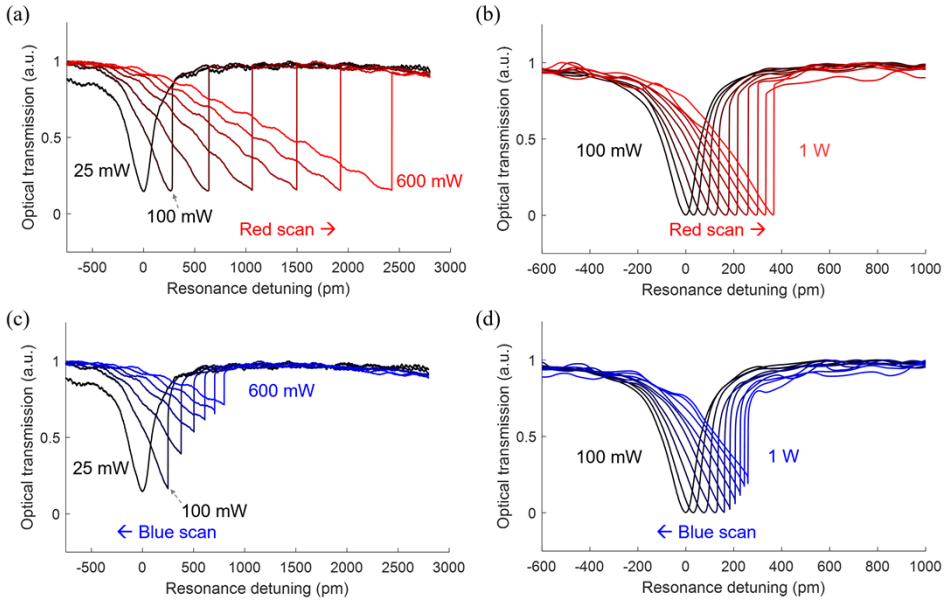

Fig. 3. Optical bi-stability response induced by scanning the laser wavelength across the cavity resonance. Increased resonance detuning and profile distortion with increased optical power to VGC (100 mW steps) (a) suspended resonator red scan response (b) SiCOI resonator red scan response (c) suspended resonator blue scan response (d) SiCOI resonator blue scan response.

SiC waveguide is higher and more concentrated than the SiCOI waveguide. This is attributed to a combination of smaller thermal conductivity of air than SiO_2 and a larger absorption rate of suspended waveguide. The thermal nonlinear index in suspended SiC waveguides could be increased by adjusting the density of crystal growth defects within the waveguide [9,33]. Ultimately there is a trade-off between a higher thermal nonlinear index and decreased waveguide propagation loss. On the contrary, by employing SiCOI, the thermal nonlinear index is around one order of magnitude lower than silicon (2×10^{-15} m^2/W) [34], showing its potential for linear devices. Moreover, we estimate the thermal nonlinear index of a suspended microring in SiCOI platform made by undercutting the SiO_2 cladding, will be larger than the non-suspended SiCOI platform, due to a lower thermal conductivity of air in comparison with SiO_2 cladding [43].

When the optical power in the waveguide reaches the optical bi-stability threshold [22], the microring resonators can exhibit two stable states for the same input optical power, which can be observed as a hysteresis loop. To measure the optical hysteresis in 3C-SiC resonators, a laser with a fixed wavelength, red detuned from the resonance wavelength, is launched into suspended and SiCOI cavities. An EDFA is used before the input of the resonator to increase the optical power, and the transmitted optical power is monitored at the output of the resonator using an optical power meter. The resultant hysteresis loops for these resonators are shown in Fig. 5 for varied detunings. It was found that the hysteresis curves are determined by the magnitude of laser detuning from resonance. Similar to silicon-based photonic cavities [9,22], the hysteresis of SiC resonators grows with the increasing detuning. The SiCOI resonator, with a smaller thermal nonlinear index, requires a higher power to show the hysteresis loop. Note that the combination of two nonlinear refractive index change effects, such as the photothermal nonlinear effect in combination with the free carrier dispersion effect in silicon resonator [44] and with TPA in graphene coating [45], could lead to the divergent curves of the hysteresis loop even at

Optics EXPRESS

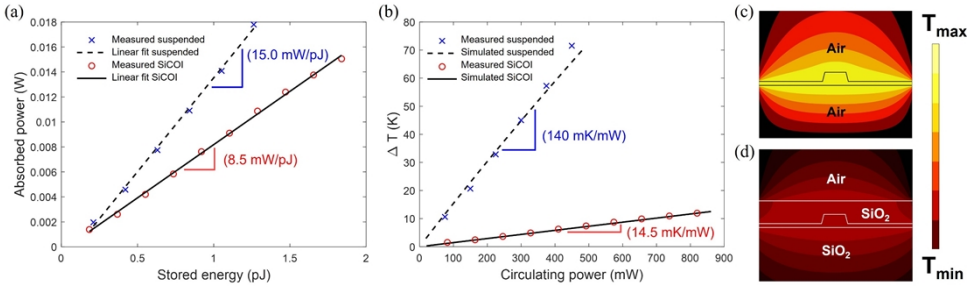

Fig. 4. Cavity absorption and temperature analysis. (a) Absorbed optical power for varied stored energy in suspended and SiCOI resonators. (b) Temperature change (ΔT) against circulating optical power for the suspended and SiCOI resonators. Simulated thermal heat distribution in (c) suspended and (d) SiCOI waveguides.

the stable region. In our case, the small opening of the hysteresis loop is only observed in the SiCOI microring resonator. This might be originated from the combination of the dominated photothermal nonlinear effect and an extra nonlinear effect resulting from the silicon-rich SiO_2 layer [5].

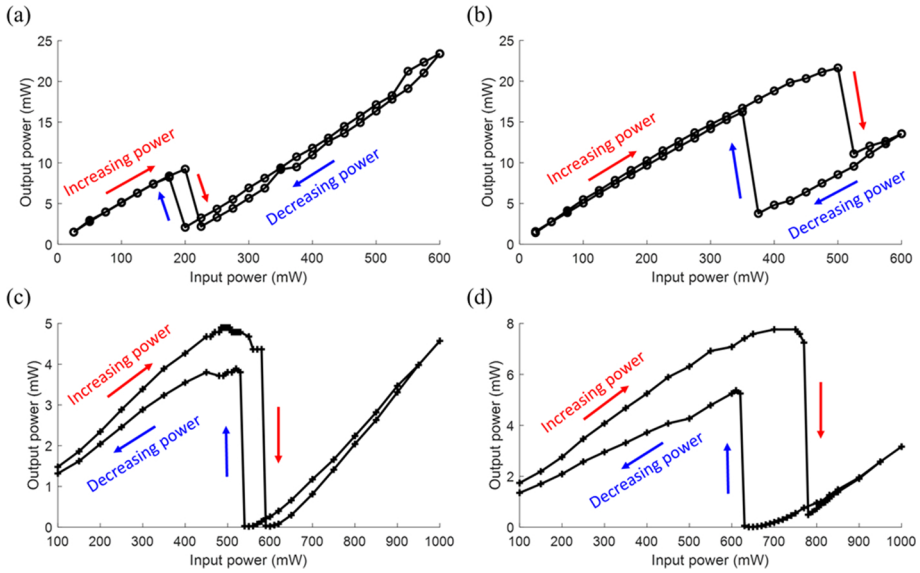

Fig. 5. Measured optical induced hysteresis in the resonators for varying input pump powers to VGC at a fixed laser wavelength red detuned from the 3C-SiC cavity resonance. (a) suspended resonator 300 pm red detuning (b) suspended resonator 500 pm red detuning (c) SiCOI resonator 200 pm red detuning (d) SiCOI resonator 250 pm red detuning.

Based on the steady-state solution of the coupled-mode equations [46,47], the resonance wavelength shift ($\Delta\lambda$) as a result of thermal-induced temperature equilibrium between the absorbed and dissipated heat in 3C-SiC resonator, is expressed as

$$\Delta\lambda = R\tau_1^{-1}\frac{\lambda_0^2 Q_I}{2\pi cn}\frac{\partial n}{\partial T}\frac{K\eta P_{in}}{(2(\lambda-\lambda_0-\Delta\lambda)/B)^2+1} \tag{1}$$

Optics EXPRESS

where λ_0 is the laser wavelength, c is the light vacuum speed, n is the refractive index of 3C-SiC, B is the FWHM of the resonance, $\frac{\partial n}{\partial T}$ is the thermal-optic coefficient, P_{in} is the input power, and K describes the fractional depth of the resonance dip under different coupling conditions [48]. Equation (1) contains more than one solution at a certain laser wavelength for given input power, further proving the existence of optical bi-stable states. To further quantify the optical bi-stability, we calculate the maximum detuning of the suspended and SiCOI resonators in the red and blue scans at various laser input power based on Eq. (1). The resonators used in the calculation have the same propagation loss, VGC loss, waveguide geometry and ring circumference as these used in the experiment, while the gaps between bus and ring waveguides are adjusted to control the circulating power within the resonators.

Figures 6(a) and 6(b) respectively show the calculated maximum detuning of the suspended and SiCOI resonators based on Eq. (1) at different optical power and coupling gaps between bus and ring waveguides in both red and blue scans, where the change of the gap will vary the FWHM and extinction ratio of the resonator [49]. The suspended platform shows a larger detuning than the SiCOI one, due to the higher linear absorption rate and the larger thermal resistance. At the same input power, the magnitude of the maximum detuning as the coupling gap increases

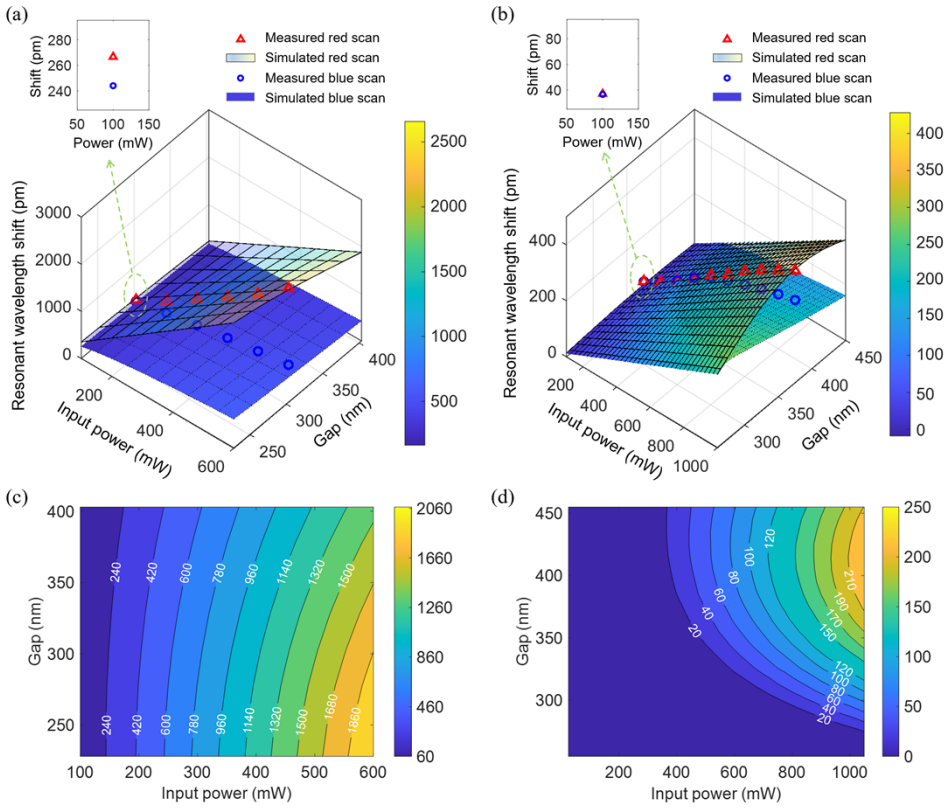

Fig. 6. Calculated maximum resonant wavelength detuning at different input optical power to VGC and coupling gap in red and blue scan for the (a) suspended resonator and (b) SiCOI resonator. Measured results are depicted in red triangulars and blue circles for red and blue scans, respectively. Insets show the zoom-in view of the measured results at an input optical power of 100 mW. Calculated difference of maximum resonant wavelength detuning in red and blue scans at different input optical power and coupling gap for the (c) suspended resonator and (d) SiCOI resonator.

Optics EXPRESS

shows a monotonical decrease and a parabolic shape for the suspended and SiCOI resonators, respectively. The top of the parabolic shape occurs when the SiCOI resonator reaches the critical coupling condition [20], while the larger propagation loss (~ 52 dB/cm) of the suspended resonator prevents this condition. Experimental results obtained for the suspended and SiCOI resonators are also shown in Figs. 6(a) and 6(b), respectively, which have a good agreement with the calculations. Moreover, the overlap between the detuning surfaces means the amounts of detuning in the red and blue scans are the same, i.e., there is no bi-stability effect. The contour plots of the calculated difference of maximum resonant wavelength detuning in red and blue scans for suspended and SiCOI resonators at different input optical power and coupling gaps are shown in Figs. 6(c) and 6(d), respectively. Due to the low threshold of the bi-stability in the suspended resonator, no overlap is observed in Fig. 6(a), and further verified in Fig. 6(c), while the SiCOI resonator exhibits an overlap as the gap increases or/and the optical power decreases, as shown in Figs. 6(b) and 6(d). These results provide a guideline to tailor the bi-stability effect for different applications.

3. Conclusions

We observe, characterize and quantify photothermal nonlinear response in 3C-SiC waveguides. We use suspended and SiCOI platforms for comparison of bi-stability due to varying amounts of optical absorption. Using the fabricated microring resonators in both platforms, we are able to characterize the photothermal nonlinear index and bi-stable behavior under various optical pump powers. Our results show the suspended and SiCOI waveguides have photothermal nonlinear coefficients of 4.02×10^{-15} m^2/W and 4.32×10^{-16} m^2/W, respectively, where the latter is one order of magnitude smaller than the photothermal nonlinear coefficient observed in Si waveguides. By using CMT to model the bi-stable behavior of the microring cavities, we are able to engineer the bi-stability for high power or nonlinear applications. Enhanced bi-stability in suspended SiC can be used for all-optical processing such as memory and logic gates; SiCOI platform will help mitigate the effects of bi-stability. By improving the crystal quality in the SiCOI waveguide fabrication process to reduce optical absorption, we envision the photothermal nonlinear index of SiCOI waveguide can be further reduced. This provides great potential for applications such as microwave photonics, frequency comb and nonlinear conversion.

Funding. University of Sydney (Research Training Program Scholarship, Sydney Research Accelerator Fellowship); Natural Sciences and Engineering Research Council of Canada.

Acknowledgments. We thank Dr L. Nguyen for discussions on device characterization. This work was carried out at the Harvard Center for Nanoscale Systems (CNS), a member of the National Nanotechnology Coordinated Infrastructure (NNCI), and the University of Sydney. J. W. and D. M. acknowledge the support of Research Training Program Scholarships from the University of Sydney. N. S. acknowledges the support of the Natural Sciences and Engineering Research Council of Canada (NSERC), the AQT Intelligent Quantum Networks and Technologies (INQNET) research program, and NSF STC "Center for Integrated Quantum Materials" under Cooperative Agreement No. DMR-1231319. M. L. acknowledges support from the Airforce Office of Scientific Research (AFOSR) under grant FA9550-19-1-0376.

Disclosures. The authors declare that there are no conflicts of interest related to this article.

Data availability. Data underlying the results presented in this paper are not publicly available at this time but may be obtained from the authors upon reasonable request.

References

1. M. A. Guidry, K. Y. Yang, D. M. Lukin, A. Markosyan, J. Yang, M. M. Fejer, and J. Vučković, "Optical parametric oscillation in silicon carbide nanophotonics," Optica **7**(9), 1139–1142 (2020).
2. D. M. Lukin, C. Dory, M. A. Guidry, K. Y. Yang, S. D. Mishra, R. Trivedi, M. Radulaski, S. Sun, D. Vercruysse, G. H. Ahn, and J. Vučković, "4H-silicon-carbide-on-insulator for integrated quantum and nonlinear photonics," Nat. Photonics **14**(5), 330–334 (2020).
3. C. Wang, Z. Fang, A. Yi, B. Yang, Z. Wang, L. Zhou, C. Shen, Y. Zhu, Y. Zhou, R. Bao, Z. Li, Y. Chen, K. Huang, J. Zhang, Y. Cheng, and X. Ou, "High-Q microresonators on 4H-silicon-carbide-on-insulator platform for nonlinear photonics," Light: Sci. Appl. **10**(1), 139 (2021).

Optics EXPRESS

4. M. A. Guidry, D. M. Lukin, K. Y. Yang, R. Trivedi, and J. Vučković, "Quantum optics of soliton microcombs," Nat. Photonics **16**(1), 52–58 (2022).
5. K. Powell, L. Li, A. Shams-Ansari, J. Wang, D. Meng, N. Sinclair, J. Deng, M. Lončar, and X. Yi, "Integrated silicon carbide electro-optic modulator," Nat. Commun. **13**(1), 1851 (2022).
6. B. Lienhard, T. Schröder, S. Mouradian, F. Dolde, T. T. Tran, I. Aharonovich, and D. Englund, "Bright and photostable single-photon emitter in silicon carbide," Optica **3**(7), 768–774 (2016).
7. S. Castelletto, A. Peruzzo, C. Bonato, B. C. Johnson, M. Radulaski, H. Ou, F. Kaiser, and J. Wrachtrup, "Silicon carbide photonics bridging quantum technology," ACS Photonics **9**(5), 1434–1457 (2022).
8. C. Babin, R. Stöhr, N. Morioka, T. Linkewitz, T. Steidl, R. Wörnle, D. Liu, E. Hesselmeier, V. Vorobyov, A. Denisenko, M. Hentschel, C. Gobert, P. Berwian, G. V. Astakhov, W. Knolle, S. Majety, P. Saha, M. Radulaski, N. T. Son, J. Ul-Hassan, F. Kaiser, and J. Wrachtrup, "Fabrication and nanophotonic waveguide integration of silicon carbide colour centres with preserved spin-optical coherence," Nat. Mater. **21**(1), 67–73 (2022).
9. K. Powell, A. Shams-Ansari, S. Desai, M. Austin, J. Deng, N. Sinclair, M. Lončar, and X. Yi, "High-Q suspended optical resonators in 3C silicon carbide obtained by thermal annealing," Opt. Express **28**(4), 4938–4949 (2020).
10. X. Lu, J. Y. Lee, S. Rogers, and Q. Lin, "Optical Kerr nonlinearity in a high-Q silicon carbide microresonator," Opt. Express **22**(25), 30826–30832 (2014).
11. P. Xing, D. Ma, K. J. A. Ooi, J. W. Choi, A. M. Agarwal, and D. Tan, "CMOS-compatible PECVD silicon carbide platform for linear and nonlinear optics," ACS Photonics **6**(5), 1162–1167 (2019).
12. D. O. Bracher and E. L. Hu, "Fabrication of high- Q nanobeam photonic crystals in epitaxially grown 4H-SiC," Nano Lett. **15**(9), 6202–6207 (2015).
13. B.-S. Song, T. Asano, S. Jeon, H. Kim, C. Chen, D. D. Kang, and S. Noda, "Ultrahigh-Q photonic crystal nanocavities based on 4H silicon carbide," Optica **6**(8), 991–995 (2019).
14. T. Fan, X. Wu, A. A. Eftekhar, M. Bosi, H. Moradinejad, E. V. Woods, and A. Adibi, "High-quality integrated microdisk resonators in the visible-to-near-infrared wavelength range on a 3C-silicon carbide-on-insulator platform," Opt. Lett. **45**(1), 153–156 (2020).
15. X. Shi, W. Fan, Y. Lu, A. K. Hansen, M. Chi, A. Yi, X. Ou, K. Rottwitt, and H. Ou, "Polarization and spatial mode dependent four-wave mixing in a 4H-silicon carbide microring resonator," APL Photonics **6**(7), 076106 (2021).
16. T. Carmon, L. Yang, and K. J. Vahala, "Dynamical thermal behavior and thermal self-stability of microcavities," Opt. Express **12**(20), 4742–4750 (2004).
17. X. Jiang and L. Yang, "Optothermal dynamics in whispering-gallery microresonators," Light: Sci. Appl. **9**(1), 2047–7538 (2020).
18. T. Tanabe, M. Notomi, S. Mitsugi, A. Shinya, and E. Kuramochi, "Fast bistable all-optical switch and memory on a silicon photonic crystal on-chip," Opt. Lett. **30**(19), 2575–2577 (2005).
19. K. Guo, L. Yang, X. Shi, X. Liu, Y. Cao, J. Zhang, X. Wang, J. Yang, H. Ou, and Y. Zhao, "Nonclassical optical bistability and resonance-locked regime of photon-pair sources using silicon microring resonator," Phys. Rev. Appl. **11**(3), 034007 (2019).
20. C. Qiu, Y. Yang, C. Li, Y. Wang, K. Wu, and J. Chen, "All-optical control of light on a graphene-on-silicon nitride chip using thermo-optic effect," Sci. Rep. **7**(1), 1–7 (2017).
21. Y. S. Duh, Y. Nagasaki, Y. L. Tang, P. H. Wu, H. Y. Cheng, T. H. Yen, H. X. Ding, K. Nishida, I. Hotta, J. H. Yang, Y. P. Lo, K. P. Chen, K. Fujita, C. W. Chang, K. H. Lin, J. Takahara, and S. W. Chu, "Giant photothermal nonlinearity in a single silicon nanostructure," Nat. Commun. **11**(1), 1–9 (2020).
22. R. Shankar, I. Bulu, R. Leijssen, and M. Lončar, "Study of thermally-induced optical bistability and the role of surface treatments in Si-based mid-infrared photonic crystal cavities," Opt. Express **19**(24), 24828–24837 (2011).
23. D. Marpaung, J. Yao, and J. Capmany, "Integrated microwave photonics," Nat. Photonics **13**(2), 80–90 (2019).
24. P. Ghelfi, F. Laghezza, F. Scotti, G. Serafino, A. Capria, S. Pinna, D. Onori, C. Porzi, M. Scaffardi, A. Malacarne, V. Vercesi, E. Lazzeri, F. Berizzi, and A. Bogoni, "A fully photonics-based coherent radar system," Nature **507**(7492), 341–345 (2014).
25. W. Bogaerts, D. Pérez, J. Capmany, D. A. B. Miller, J. Poon, D. Englund, F. Morichetti, and A. Melloni, "Programmable photonic circuits," Nature **586**(7828), 207–216 (2020).
26. V. R. Almeida and M. Lipson, "Optical bistability on a silicon chip," Opt. Lett. **29**(20), 2387–2389 (2004).
27. C. Baker, S. Stapfner, D. Parrain, S. Ducci, G. Leo, E. M. Weig, and I. Favero, "Optical instability and self-pulsing in silicon nitride whispering gallery resonators," Opt. Express **20**(27), 29076–29089 (2012).
28. P. Xing, D. Ma, L. C. Kimerling, A. M. Agarwal, and D. T. H. Tan, "High efficiency four wave mixing and optical bistability in amorphous silicon carbide ring resonators," APL Photonics **5**(7), 076110 (2020).
29. X. Shi, W. Fan, A. K. Hansen, M. Chi, A. Yi, X. Ou, K. Rottwitt, and H. Ou, "Thermal behaviors and optical parametric oscillation in 4H-silicon carbide integrated platforms," Adv. Photonics Res. **2**(10), 2100068 (2021).
30. X. Tang, K. G. Irvine, D. Zhang, and M. G. Spencer, "Linear electro-optic effect in cubic silicon carbide," Appl. Phys. Lett. **59**(16), 1938–1939 (1991).
31. J. Cardenas, M. Zhang, C. T. Phare, S. Y. Shah, C. B. Poitras, B. Guha, and M. Lipson, "High-Q SiC microresonators," Opt. Express **21**(14), 16882–16887 (2013).
32. T. Fan, H. Moradinejad, X. Wu, A. A. Eftekhar, and A. Adibi, "High-Q integrated photonic microresonators on 3C-SiC-on-insulator (SiCOI) platform," Opt. Express **26**(20), 25814–25826 (2018).
33. F. Martini and A. Politi, "Linear integrated optics in 3C silicon carbide," Opt. Express **25**(10), 10735–10742 (2017).

Optics EXPRESS

34. C. Horvath, D. Bachman, R. Indoe, and V. Van, "Photothermal nonlinearity and optical bistability in a graphene–silicon waveguide resonator," Opt. Lett. **38**(23), 5036–5039 (2013).
35. K. Ikeda, R. E. Saperstein, N. Alic, and Y. Fainman, "Thermal and Kerr nonlinear properties of plasma-deposited silicon nitride/silicon dioxide waveguides," Opt. Express **16**(17), 12987–12994 (2008).
36. B. Desiatov, A. Shams-Ansari, M. Zhang, C. Wang, and M. Lončar, "Ultra-low-loss integrated visible photonics using thin-film lithium niobate," Optica **6**(3), 380–384 (2019).
37. C. Schmidt, A. Chipouline, T. Pertsch, A. Tünnermann, O. Egorov, F. Lederer, and L. Deych, "Nonlinear thermal effects in optical microspheres at different wavelength sweeping speeds," Opt. Express **16**(9), 6285–6301 (2008).
38. D. Talwar and J. Sherbondy, "Thermal expansion coefficient of 3C–SiC," Appl. Phys. Lett. **67**(22), 3301–3303 (1995).
39. X. Xue, Y. Xuan, C. Wang, P.-H. Wang, Y. Liu, B. Niu, D. E. Leaird, M. Qi, and A. M. Weiner, "Thermal tuning of Kerr frequency combs in silicon nitride microring resonators," Opt. Express **24**(1), 687–698 (2016).
40. M. Borselli, T. J. Johnson, and O. Painter, "Beyond the Rayleigh scattering limit in high-Q silicon microdisks: theory and experiment," Opt. Express **13**(5), 1515–1530 (2005).
41. M. Borselli, T. J. Johnson, and O. Painter, "Accurate measurement of scattering and absorption loss in microphotonic devices," Opt. Lett. **32**(20), 2954–2956 (2007).
42. F. Ramiro-Manzano, N. Prtljaga, L. Pavesi, G. Pucker, and M. Ghulinyan, "Thermo-optical bistability with Si nanocrystals in a whispering gallery mode resonator," Opt. Lett. **38**(18), 3562–3565 (2013).
43. M. Soltani, Q. Li, S. Yegnanarayanan, and A. Adibi, "Improvement of thermal properties of ultra-high Q silicon microdisk resonators," Opt. Express **15**(25), 17305–17312 (2007).
44. G. Priem, P. Dumon, W. Bogaerts, D. V. Thourhout, G. Morthier, and R. Baets, "Optical bistability and pulsating behaviour in Silicon-On-Insulator ring resonator structures," Opt. Express **13**(23), 9623–9628 (2005).
45. Y. Gao, W. Zhou, X. Sun, H. K. Tsang, and C. Shu, "Cavity-enhanced thermo-optic bistability and hysteresis in a graphene-on-Si3N4 ring resonator," Opt. Lett. **42**(10), 1950–1953 (2017).
46. B. E. Little, S. T. Chu, H. A. Haus, J. Foresi, and J. P. Laine, "Microring resonator channel dropping filters," J. Lightwave Technol. **15**(6), 998–1005 (1997).
47. R. R. Galiev, N. M. Kondratiev, V. E. Lobanov, A. B. Matsko, and I. A. Bilenko, "Mirror-assisted self injection locking of a laser to a Whispering-Gallery-Mode microresonator," Phys. Rev. Appl. **16**(6), 064043 (2021).
48. M. L. Gorodetsky and V. S. Ilchenko, "Optical microsphere resonators: optimal coupling to high-Q whispering-gallery modes," J. Opt. Soc. Am. B **16**(1), 147–154 (1999).
49. W. Bogaerts, P. De Heyn, T. Van Vaerenbergh, K. De Vos, S. Kumar Selvaraja, T. Claes, P. Dumon, P. Bienstman, D. Van Thourhout, and R. Baets, "Silicon microring resonators," Laser Photonics Rev. **6**(1), 47–73 (2012).